Model Predictive Path-Planning Controller With Potential Function for Emergency Collision Avoidance on Highway Driving

Pengfei Lin and Manabu Tsukada, *Member, IEEE*

***Abstract*—Existing potential functions (PFs) utilized in autonomous vehicles mainly focus on solving the path-planning problems in some conventional driving scenarios; thus, their performance may not be satisfactory in the context of emergency obstacle avoidance. Therefore, we propose a novel model predictive path-planning controller (MPPC) combined with PFs to handle complex traffic scenarios (e.g., emergency avoidance when a sudden accident occurs). Specifically, to enhance the safety of the PFs, we developed an MPPC to handle an emergency case with a sigmoid-based safe passage embedded in the MPC constraints (SPMPC) with a specific triggering analysis algorithm on monitoring traffic emergencies. The presented PF-SPMPC algorithm was compiled in a comparative simulation study using MATLAB/Simulink and CarSim. The algorithm outperformed the latest PF-MPC approach to eliminate the severe tire oscillations and guarantee autonomous driving safety when handling the traffic emergency avoidance scenario.**

***Index Terms*—Autonomous vehicles, model predictive control, potential function, path planning, collision avoidance.**

NOMENCLATURE

$\{X, Y\}$	Global coordinate of ego-vehicle
$\{X^i_{obs}, Y^i_{obs}\}$	Global coordinate of i^{th} obstacle
ζ	Scaling factor of road PF
$Y_{u,l}$	Lateral position of road's upper and lower boundary
l_w	Width of the vehicle
A_c	Maximum amplitude of the lane divider potential
Y^j_c	Lateral position of the j^{th} lane division
λ	Inclination of the lane's potential power
A_{obs}	Maximum amplitude of the obstacle potential
$\sigma^i_{x,y}$	Longitudinal and lateral factors of ith obstacle's PF
D_h	Relative braking distance
P	Minimal positive factor
V, V^i_{obs}	Longitudinal speed of ego-vehicle & i^{th} obstacle
a_{brake}	Deceleration of the ego and obstacle vehicle
$l_{fr}, l^i_{fr,obs}$	Length of the ego and i^{th} obstacle vehicle
β	Sideslip angle of ego-vehicle
$\psi, \dot{\psi}$	Yaw angle Yaw rate of ego-vehicle
$C_{f,r}$	Cornering stiffness of (front, rear) tires
$l_{f,r}$	Longitudinal distance from c.g. to (front, rear) tires
m	Total mass of vehicle
I_z	Yaw moment of inertia of ego-vehicle
$N_{P,C}$	Prediction and control horizons of the MPC
T	Sampling time
δ_f	Front tire steering angle of ego-vehicle
W_s	Lane width of the road
ρ	slope of the sigmoid-based SP at the central symmetry point
$P_{x,y}$	Parameters related to the start position of vehicle lane change
Y^{lane}_u	Lateral position of upper lane centerline
ϵ	Minimum positive shifting factor

Manuscript received September 8, 2021; accepted February 7, 2022. Date of publication February 22, 2022; date of current version March 1, 2022. This letter was recommended for publication by Associate Editor J. Yu and Editor S. J. Guy upon evaluation of the reviewers' comments. This work was supported by JSPS KAKENHI under Grants 19KK0281 and 21H03423. *(Corresponding author: Pengfei Lin.)*

The authors are with the Department of Creative Informatics, Graduate School of Information Science and Technology, The University of Tokyo, Tokyo 113-8657, Japan (e-mail: linpengfei0609@gmail.com; mtsukada@g.ecc.u-tokyo.ac.jp).

Digital Object Identifier 10.1109/LRA.2022.3152693

I. Introduction

In RECENT years, researchers from both industry and academia have attempted to develop autonomous driving technologies that can ensure better safety during daily travel. However, research on autonomous vehicles has encountered some obstacles because experimental road tests have caused major accidents. These safety issues have drawn public attention to the fact that current autonomous vehicles cannot guarantee safety in dangerous situations (e.g., inclement weather conditions, uneven pavement, and sudden obstacles). Thus, accurate perception and path planning are the two cardinal requirements for safe autonomous driving, which were promoted by several autonomous driving projects, such as DARPA Urban Challenge [1], Grand Cooperative Driving Challenge (GCDC) project [2], etc. Safety planning has been recently stressed in autonomous vehicles, e.g., interactive planning considering risk-averse decisions is used for adversarial scenarios [3], and probabilistic planning with safety assurance is proposed in the traffic weaving scenario for human-robot vehicle interactions [4]. To expand the safety planning for emergency scenarios, potential functions (PFs), which model the 3D risk field for real-time path generation, become one of the mainstream planning algorithms in the current research focus [5]. PFs are initially implemented

in robotic path planning because of their simplicity and real-time computation in collision avoidance. Besides, the PFs are similar to the feedback control strategy that can directly obtain control inputs or constraints for optimization algorithms like model predictive control (MPC) [6]. They can simultaneously establish a repulsive and an attractive potential field for surrounding obstacles and goal points, respectively. The path is generated along the direction of gradient descent [7]. With the development of autonomous driving technology, researchers have attempted to implement PFs in self-driving vehicles because the fast computation of PFs satisfies the requirement for the lower control system to act in real time. Currently, research is progressing in two main directions. One concerns the use of PFs as a hazard evaluation assessment or penalty term to reduce the potential risk of crashing with other vehicles [8]–[10], and the other involves the use of PFs as part of a path-planning algorithm to generate paths along the gradient descent directly while maintaining fast computation [11], [13], [14].

In the domain of path planning, the functions used for PF design are research highlights. Specifically, the exponential and trigonometric functions are utilized instead of the quadratic function [17], [18]. In [11], [12], a multi-constraint model predictive controller (MMPC) was designed to produce trackable paths by directly adding constraints to path generation, such as the gradient angle. However, this cannot ensure safety when the PFs require a large gradient angle to avoid a sudden obstacle. In a recent study [14], two potential fields contained a novel potential velocity field to denote the longitudinal and lateral accelerations of the surrounding vehicles. However, traffic emergencies like emergency braking and lane change of surrounding vehicles were not considered in this study. In [21], a sigmoid curve was applied to generate path candidates for hybrid path planning when the PFs could not find the shortest path. However, the obstacle vehicle's speed was constant, and the computation time increased because another optimization function had to be designed to select the optimal path. later, [15], [16] combines the clothoidal curve with the PFs to consider vehicle dynamics and real world traffic data for emergency collision avoidance in the process of path generation, but only single driving scenario is simulated in the comparative study. For considering multiple obstacle vehicles on the highway, [19] proposes an adaptive PFs-based model predictive controller by overlapping two Gaussian probability density functions to compute the 3D risk field more accurately, but only straight-ahead obstacle vehicles that maintain a long Euclidean distance were considered in this study. In general, prior studies have one common limitation: emergency avoidance due to unexpected deceleration of the obstacle vehicle has not been considered. Thus, the inherent limitations of PFs [20], [22], such as oscillations in narrow passages, have not been discussed.

To guarantee the safety of PFs even in traffic emergencies, we propose a novel model predictive path-planning controller (MPPC) with a built-in safe passage (SP) to handle situations where PFs fail to plan a safe and smooth path when the front obstacle vehicle suddenly decelerates. The sudden deceleration of the obstacle vehicle will cause a sharp increase in the potential field, which will partially overlap with the potential fields of other obstacles, generating the narrow passage mentioned in [22]. Therefore, we use a sigmoid-like function to design the SP considering the traffic emergency. Furthermore, we compute a triggering estimation algorithm to monitor the traffic emergency; this algorithm determines whether to trigger the SP constraint, as shown in Fig. 1. The proposed PF-SPMPC method was simulated in a comparative emergency scenario, wherein it was compared with the latest adaptive PF-based MPC (PF-AMPC) approach [19] under co-simulation in MATLAB/Simulink and CarSim. The results show that the proposed method outperforms the latest approach in eliminating severe oscillations when passing through a narrow passage.

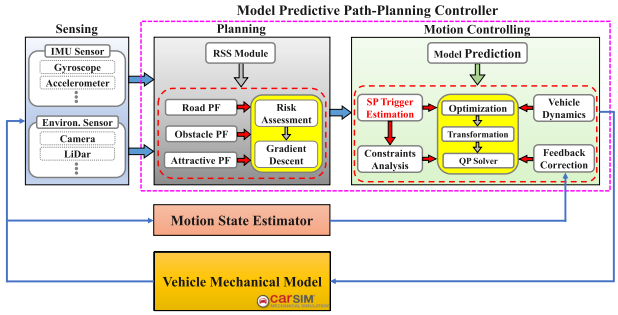

Fig. 1. Overall framework of SP-based model predictive path-planning system.

The remainder of this paper is organized as follows: First, a detailed description of the planning module for collision avoidance is presented in Section II, including the PF design and gradient descent method. In section III, a vehicle lateral dynamics model is introduced for model prediction, and the derivation of the model predictive controller is presented in detail, which includes the SP, constraint analysis, and optimization formulation. Section IV describes the overall simulation environment settings and verifies the superiority of the proposed method. Finally, the conclusions and future research directions are presented in Section V.

II. Planning: Potential Functions With Collision Avoidance

In this section, the PFs in the planning module for vehicle collision avoidance are introduced in detail.

A. Road Potential Functions

Normally, the road structure is composed of road boundaries, road centerlines, and lane markings. Therefore, the road PFs representing the potential power of the boundaries and centerlines are utilized to keep the vehicle driving within the road; these PFs are expressed as [17]:

$$P_{RB} = \frac{1}{2}\zeta\left(\frac{1}{Y - Y_{u,l} - l_w/2}\right)^2, \tag{1}$$

$$P_{RC}^{j} = A_c \exp\left(\frac{(Y - Y_c^j)^2}{2\lambda^2}\right), \tag{2}$$

where $j = 1, 2, \ldots, L$ indicates the index of each lane division. In this study, we assume that the lanes have the same dimension and consider a road structure with at most three lanes in the same driving direction.

B. Obstacle Potential Function

The design of the obstacle PF considers two aspects: one is to keep the ego-vehicle a certain safe distance away from the obstacle vehicle, and the other is to guide the ego-vehicle during lane changes [18]. Therefore, we modify the obstacle PF to consider the static and dynamic obstacles, as follows:

$$P_{OB}^{i} = A_{obs} \exp\left(-\left(\frac{(X - X_{obs}^{i})^2}{2(\sigma_x^i)^2} + \frac{(Y - Y_{obs}^{i})^2}{2(\sigma_y^i)^2}\right)\right), \tag{3}$$

where

$$\sigma_y^i = \begin{cases} \frac{l_w\left[\cos\left(\frac{X - X_{obs}^{i} + D_h}{D_h}\pi\right) + 1\right]}{-8\left[\sigma_x\left(X - X_{obs}^{i}\right)^2 + \ln(P)\right]} & , |X - X_{obs}^{i}| \le D_h \\ 0 & , |X - X_{obs}^{i}| > D_h, \end{cases}$$

$$\sigma_x^i = \sqrt{-\frac{D_h^2}{2\ln(\frac{P}{A_{obs}})}},$$

$$D_h = \begin{cases} \frac{V^2}{2a_{brake}} + \frac{l_{fr} + l_{fr,obs}^{i}}{2} & , V_{obs}^{i} = 0 \\ \frac{V^2 - (V_{obs}^{i})^2}{2a_{brake}} + \frac{l_{fr} + l_{fr,obs}^{i}}{2} + d_{\min} & , V_{obs}^{i} \neq 0. \end{cases}$$

where $i = 1, \ldots, M$ denotes the index of each obstacle and d_{min} is the minimum safe distance from the responsibility-sensitive safety (RSS) model [26], [27]. σ_x^i and σ_y^i determine the shape of the obstacle's PF based on the relative speed and distance between the ego-vehicle and the obstacle. (3) can handle most different types of cars (e.g., sedan and SUV). We superimposed the aforementioned PFs and calculated the corresponding directional force by applying the gradient descent method:

$$F_{TO} = -\nabla P_{TO} = -\begin{bmatrix} \frac{\partial P_{TO}}{\partial X} & \frac{\partial P_{TO}}{\partial Y} \end{bmatrix}^T, \tag{4}$$

where

$$P_{TO} = P_{RB} + \sum_{j=1}^{L} P_{RC}^{j} + \sum_{i=1}^{M} P_{OB}^{i}.$$

The potential field of the road defined from (1) to (3) is illustrated in Fig. 3.

III. Motion Control: Model Predictive Path-Planning Controller

In this section, the derivation of the SP-based model predictive controller (SPMPC) that formalizes a real-time optimization problem is presented in depth, including vehicle motion modeling, future prediction of model outputs, constraints analysis, and optimization design.

A. Vehicle Dynamics Modeling

The vehicle dynamics model utilized as a predictive model in MPC is depicted in Fig. 2. The vehicle motion states are chosen as follows:

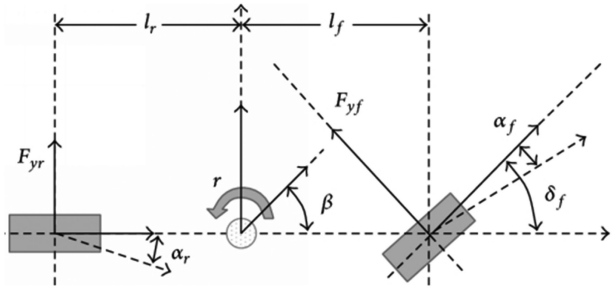

Fig. 2. Vehicle lateral dynamics model [23], [24].

$$\mathbf{x}(k) = \begin{bmatrix} Y & \beta & \psi & \dot{\psi} \end{bmatrix}^T, \tag{5}$$

According to [25, pp. 398–430], F_{xf} and F_{xr} can be approximated by the Magic Formula; then the lateral and yaw dynamics can be described as

$$\dot{\beta} = \frac{-(C_r + C_f)}{mV}\beta + \left(\frac{C_r l_r - C_f l_f}{mV^2} - 1\right)\dot{\psi} + \frac{C_f}{mV}\delta_f, \tag{6}$$

$$\ddot{\psi} = \frac{C_r l_r - C_f l_f}{I_z}\beta + \left(\frac{C_r l_r^2 + C_f l_f^2}{I_z V}\dot{\psi} + \frac{C_f l_f}{I_z}\delta_f. \right. \tag{7}$$

With a control sampling period T, discretization using a zero-order hold (ZOH) equivalence sampling rate of $1/T$ yields the discrete-time linear vehicle model with the control input δ_f for the MPC design, which can be expressed as

$$\mathbf{x}(k+1) = \Phi\mathbf{x}(k) + \Gamma u(k) \tag{8}$$

$$\mathbf{y}(k) = C\mathbf{x}(k) \tag{9}$$

where

$$\Phi = \begin{bmatrix} 1 & TV & TV & 0 \\ 0 & -\frac{(C_r + C_f)T}{mV} + 1 & 0 & \frac{(C_r l_r - C_f l_f)T}{mV^2} - T \\ 0 & 0 & 1 & T \\ 0 & \frac{C_r l_r - C_f l_f}{I_z}T & 0 & -\frac{C_r l_r^2 + C_f l_f^2}{I_z V}T + 1 \end{bmatrix},$$

$$\Gamma = \begin{bmatrix} 0 & \frac{C_f}{mV}T & 0 & \frac{C_f l_f}{I_z}T \end{bmatrix}^T, \quad C = \begin{bmatrix} 1 & 0 & 0 & 0 \\ 0 & 0 & 1 & 0 \end{bmatrix}.$$

B. Future Prediction of Model Outputs

First, the model described in Section II is transferred into an incremental model because the constraints on the control increment must be considered. The new state is then defined as

$$\mathbf{x}_n = \begin{bmatrix} \Delta\mathbf{x}(k) & \mathbf{y}(k) \end{bmatrix}^T \tag{10}$$

where $\Delta\mathbf{x}(k) = \mathbf{x}(k) - \mathbf{x}(k-1)$. Combining (10) with (8) and (9), the new discrete state-space model becomes

$$\mathbf{x}_n(k+1) = \Phi_n\mathbf{x}_n(k) + \Gamma_n\Delta u(k) \tag{11}$$

$$\mathbf{y}_n(k) = C_n\mathbf{x}_n(k) \tag{12}$$

where

$$\Phi_n = \begin{bmatrix} \Phi & Z_n \\ C\Phi & I_n \end{bmatrix}, \Gamma_n = \begin{bmatrix} \Gamma \\ C\Gamma \end{bmatrix}, C_n = \begin{bmatrix} Z_n \\ I_n \end{bmatrix}^T,$$
$$Z_n = \mathbf{0}_{4\times 2},\ I_n = \mathbf{1}_{2\times 2}.$$

Therefore, the future state of the vehicle can be predicted at each time step, given the current measured information $\mathbf{x}_n(k)$:

$$\mathbf{x}_n(k), \ldots, \mathbf{x}_n(k+n), \ldots, \mathbf{x}_n(k+N_p)$$

The sequence of future control inputs is denoted by

$$\Delta U(k) = \left[\Delta u(k), \ldots, \Delta u(k+m), \ldots, \Delta u(k+N_c-1)\right]$$

The derivation of the iterative prediction (shortened because of space limitations) is

$$\Xi(k) = \Theta \mathbf{x}_n(k) + \Upsilon \Delta U(k) \tag{13}$$

where

$$\Xi(k) = \left[\mathbf{y_n(k+1)} \quad \mathbf{y}_n(k+2) \quad \cdots \quad \mathbf{y}_n(k+N_p)\right]^T_{N_p\times 1},$$

$$\Theta = \left[C_n\Phi_n \quad C_n\Phi_n^2 \quad C_n\Phi_n^3 \quad \cdots \quad C_n\Phi_n^{N_p}\right]^T_{2N_p\times 6},$$

$$\Upsilon = \begin{bmatrix} C_n & 0 & \cdots & 0 \\ C_n\Phi_n\Gamma_n & C_n\Gamma_n & \cdots & 0 \\ \vdots & \vdots & \ddots & \vdots \\ C_n\Phi_n^{N_p-1}\Gamma_n & C_n\Phi_n^{N_p-2}\Gamma_n & \cdots & C_n\Phi_n^{N_p-N_c-1}\Gamma_n \end{bmatrix}_{2N_p\times N_c}$$

C. Analysis of Constraints Design for MPC

In the literature [11], the general MPC formulation is normally observed to impose constant constraints on the motion states, control input, and control input increment, which can then be expressed as

$$-F_c\Delta u_{\max} \le \Delta U \le F_c\Delta u_{\max}, \tag{14}$$

$$-F_c(u_{\max} + u(k-1)) \le S_c\Delta U \le F_c(u_{\max} - u(k-1)), \tag{15}$$

$$T_c\Xi_{\min} \le \Xi \le T_c\Xi_{\max}, \tag{16}$$

where

$$F_c = \begin{bmatrix} 1 \\ 1 \\ \vdots \\ 1 \end{bmatrix}_{N_c\times 1}, \quad S_c = \begin{bmatrix} 1 & 0 & \cdots & 0 \\ 1 & 1 & \cdots & 0 \\ \vdots & \vdots & \ddots & \vdots \\ 1 & 1 & \cdots & 1 \end{bmatrix}_{N_c\times N_c},$$

$$T_c = \begin{bmatrix} 1 & 0 & 1 & 0 & \cdots & 1 & 0 & 1 & 0 \\ 0 & 1 & 0 & 1 & \cdots & 0 & 1 & 0 & 1 \end{bmatrix}^T_{2N_p\times 2}.$$

There exists an important premise for a constraint design that ensures that the PF-based path-planning module can only be assumed to work in normal driving cases.

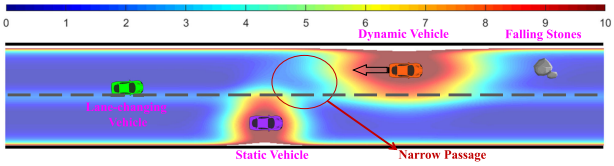

Fig. 3. 3D illustration of the road's potential field in an emergency situation.

However, we consider an emergency obstacle avoidance scenario in which we assume that the collision can only be avoided by steering instead of braking. Assume that there are two obstacle vehicles on the highway: the first one—in the same lane as the ego-vehicle—is stopped because of an engine failure, and the other is driving at a constant speed in the adjacent lane. The ego-vehicle needs to steer to avoid the first static obstacle, but the second dynamic obstacle vehicle suddenly decelerates due to an unexpected accident. This sudden deceleration will cause the obstacle's potential field to enlarge sharply in the longitudinal direction; this field would then partially overlap with the potential fields of the other vehicles. This would cause the gradient to vary abnormally, whereby the performance of the PFs will become unstable. Moreover, as concluded in Section I, the PFs will cause severe oscillations owing to abnormal changes in the gradient descent when the vehicle passes through a narrow passage [22], as depicted in Fig. 3.

To enhance the safety of the ego-vehicle in such a situation, we design a SP by utilizing a sigmoid-like function and introduce this function into the lateral position constraint design of the MPC. This function was chosen because it can calculate the upper and lower boundaries of SP relatively and smoothly with the given position information of the ego and obstacle vehicle at each time step, as expressed below:

$$S_{pas} = \frac{W_S}{1 + \exp[\rho(X^i_{obs} - X) - P_x]} + P_y, \tag{17}$$

In addition, when the ego-vehicle is not between obstacles, the longitudinal position of the sigmoid's central symmetry point is set to be equal to $X^i_{obs} - D_h$, which can enable the ego-vehicle to avoid the obstacle vehicle ahead. Therefore, the SP can be created by shifting (17) within a certain range ϵ (depending on the urgency of the situation):

$$\begin{cases} S^{lb}_{pas} = S_{pas} - \epsilon, \\ S^{ub}_{pas} = S_{pas} + \epsilon, \end{cases} \tag{18}$$

where lb and ub denote the lower and upper bound of the SP, $\epsilon \in (0, 1]$ is used to create the SP.

D. Optimization Design With Vehicle Dynamics

Two aspects need to be considered in the design of the cost function in MPC: the penalty on the path-tracking error and the requirement of a steady increase of control increment. Therefore, the cost function can be formulated as

$$J(\mathbf{x}_n(k), \Delta U(k)) = \|\Xi_{ref}(k) - \Xi(k)\|^2_Q + \|\Delta U(k)\|^2_R \tag{19}$$

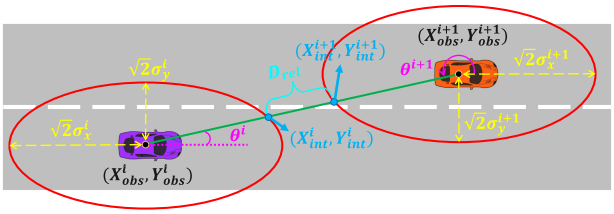

Fig. 4. Triggering analysis of the potential fields of the obstacle vehicles to determine whether a narrow passage is produced.

where $\Xi_{ref}(k) = \begin{bmatrix} \mathbf{y_{ref}(k+1)} & \cdots & \mathbf{y}_{ref}(k+N_p) \end{bmatrix}^T_{N_p \times 1}$ and $\mathbf{y}_{ref}(k+1) = \begin{bmatrix} Y_{PF}(k+1) & \psi_{PF}(k+1) \end{bmatrix}^T$ are the reference signals obtained in Section III, and Q and R are weighting matrices. (19) is then transformed into a quadratic programming problem to reduce computational time while combining it with vehicle dynamics (11)–(12) and constraints (14)–(17); the resulting expression is rearranged as

$$\min\ J = \min_{\Delta U} \frac{1}{2} \Delta U(k)^T H \Delta U(k) + \Delta U(k)^T f \tag{20}$$

$$\text{s.t.}\quad \mathbf{x}_n(k+1) = \Phi_n \mathbf{x}_n(k) + \Gamma_n \Delta u(k), \tag{20a}$$

$$\mathbf{y}_n(k) = C_n \mathbf{x}_n(k), \tag{20b}$$

$$-F_c \Delta u_{\max} \le \Delta U \le F_c \Delta u_{\max}, \tag{20c}$$

$$T_c \Xi_{\min} \le \Xi \le T_c \Xi_{\max}, \tag{20-D}$$

$$-F_c(u_{\max} + u(k-1)) \le S_c \Delta U \le F_c(u_{\max} - u(k-1)), \tag{20e}$$

$$\begin{cases} S_{pas}^{lb} \le Y \le Y_u^{lane} + \epsilon, & , X \notin (X_{obs}^i, X_{obs}^{i+1}) \\ S_{pas}^{lb} \le Y \le S_{pas}^{ub}, & , X \in [X_{obs}^i, X_{obs}^{i+1}] \end{cases}. \tag{20f}$$

where

$$H = 2(\Upsilon^T \tilde{Q} \Upsilon + \tilde{R}), \quad f = -2(\Xi_{ref}(k) - \Xi(k))^T \Upsilon,$$

$$\tilde{Q} = \text{diag}\left(\{Q_i\}_0^{N_p-1}\right), \text{ and } \tilde{R} = \text{diag}\left(\{R_i\}_0^{N_c-1}\right).$$

In inequality constraint (20f), when the ego-vehicle is not between obstacles (all the obstacles are ahead of the ego-vehicle or there is only one obstacle), only the lower bound of the SP and a constant bound above the upper lane centerline are computed to reduce computation time. When the ego-vehicle is between obstacles, both the lower and upper bound of the SP should be considered. The proposed SP constraints are depicted in Fig. 6 (the first obstacle vehicle is set on the lower lane).

Note that the constraint (20f) is only triggered when the PFs cannot plan a safe, feasible path due to an emergency, i.e., a falling stone or a suddenly appearing pedestrian. Whether to trigger an SP constraint can be determined by monitoring the degree to which the longitudinal and lateral coefficients of the PFs increase, or whether the potential fields of the obstacles overlap mutually. Herein, we propose a concise algorithm to judge whether there is an overlap between the potential fields of the obstacle vehicles. As shown in Fig. 4, we obtain a two-dimensional elliptic potential field by projecting the three-dimensional potential field of the obstacle vehicle onto the X-Y plane to simplify the analysis. From (3), we see that the projection of the potential field of the i^{th} obstacle vehicle (X_{obs}^i, Y_{obs}^i) along the Z-axis is a quasi-standard ellipse, where the long and short half-axes are $\sqrt{2}\sigma_x^i$ and $\sqrt{2}\sigma_y^i$, respectively. The ellipse of the $(i+1)^{th}$ obstacle vehicle $(X_{obs}^{i+1}, Y_{obs}^{i+1})$ can be obtained in the same manner, with $\sqrt{2}\sigma_x^{i+1}$ and $\sqrt{2}\sigma_y^{i+1}$ as the long and short half-axes, respectively. According to [28], the minimum distance D_{rel} between two ellipses can be calculated using the Euclidean distance and Lagrange multiplier to obtain the approximate solution with the conditions for an extremum. However, the computational cost of this method is extremely high. [29] provides a full analysis of the distance of two arbitrary ellipses in the two-dimensional plane; it is considered that when the two ellipses are oriented in the same direction, the connecting line between the centers of the ellipses intersects with the edges of the ellipses to produce two intersection points. Then, D_{rel} can be approximated by the distance between the two intersection points, as shown in Fig. 4. Next, to calculate D_{rel}, it is necessary to obtain the coordinate values of the two intersection points from the two ellipses that intersect with a line connecting the centers of them, denoted as (X_{int}^i, Y_{int}^i) and $(X_{int}^{i+1}, Y_{int}^{i+1})$ in Fig. 4. According to the properties of the elliptic equation, we can obtain the following equations:

$$\begin{cases} \frac{(X_{int}^i - X_{obs}^i)^2}{2(\sigma_x^i)^2} + \frac{(Y_{int}^i - Y_{obs}^i)^2}{2(\sigma_y^i)^2} = 1 \\ \tan\theta^i = \frac{Y_{int}^i - Y_{obs}^i}{X_{int}^i - X_{obs}^i} \end{cases} \tag{21}$$

where θ^i is the angle between the intersection point (X_{int}^i, Y_{int}^i) and the long half-axis of the ellipse. The second equation can be substituted into the first equation for the solution:

$$(X_{int}^i - X_{obs}^i)^2 = \frac{2(\sigma_x^i \sigma_y^i)^2}{(\sigma_y^i)^2 + (\sigma_x^i)^2 \tan^2\theta^i} \tag{22}$$

Then, considering $\theta \in (0, \frac{\pi}{2})$, we can obtain the coordinate value of (X_{int}^i, Y_{int}^i) as follows:

$$\begin{cases} X_{int}^i = \frac{\sqrt{2}\sigma_x^i \sigma_y^i}{\sqrt{\sigma_y^2 + \sigma_x^2 \tan^2\theta^i}} + X_{obs}^i \\ Y_{int}^i = \frac{\sqrt{2}\sigma_x^i \sigma_y^i \tan\theta^i}{\sqrt{(\sigma_y^i)^2 + (\sigma_x^i)^2 \tan^2\theta^i}} + Y_{obs}^i \end{cases} \tag{23}$$

It is important to note that $\tan\theta^i$ can be calculated using the positions of the obstacle vehicles:

$$\tan\theta^i = \frac{Y_{obs}^{i+1} - Y_{obs}^i}{X_{obs}^{i+1} - X_{obs}^i} \tag{24}$$

The position information of the obstacle vehicles can be accessed from onboard sensors. Therefore, we can substitute (24) into (23) to obtain the numerical value of (X_{int}^i, Y_{int}^i). We can use the same method to obtain the solutions of $(X_{int}^{i+1}, Y_{int}^{i+1})$. However, it must be noted that $\theta^{i+1} \in (\pi, \frac{3\pi}{2})$, which leads to a negative value for $\tan\theta^{i+1}$. Finally, we can calculate D_{rel}:

$$D_{rel} = \sqrt{(Y_{int}^{i+1} - Y_{int}^i)^2 + (X_{int}^{i+1} - X_{int}^i)^2} \tag{25}$$

Therefore, based on (25), we can compute an algorithm (Algorithm 1) to determine if a narrow passage exists when

TABLE I
PARAMETER SETTINGS OF POTENTIAL FIELD

	Parameter	Value	Unit
Road Potential Field	ζ	3	
	$Y_{u,l}$	8,0	meter
	l_w	1.6	meter
	A_c	2	
	Y_c	4	meter
	λ	1.2	
Obstacle Potential Field	A_{obs}	10	
	l_{fr}	3.05	meter
	P	0.01	
	a_{brake}	5	m/s^2

Algorithm 1: Triggering Estimation on SP Constraint.

Initialization:$(X^i_{int}, Y^i_{int}), (X^{i+1}_{int}, Y^{i+1}_{int}) \leftarrow (0,0)$
$T_{SP} \leftarrow$ **false**
repeat
  Update σ^i_x, σ^i_y based on (3)
  Update θ^i based on (24)
  Update X^i_{int}, Y^i_{int} based on (23)
  $\theta^{i+1} \leftarrow \theta^i + \pi$
  Update $X^{i+1}_{int}, Y^{i+1}_{int}$ based on (23)
  Update D_{rel} based on (25)
  if $D_{rel} \leq D_{thold}$ **then**
    $T_{SP} \leftarrow$ **true**
    Compute S_{pas} based on (17), (18)
    Constraint (20f) $\leftarrow$ on
    Minimize (20)
  else
    Minimize (20) without S_{pas}
  end if
until $\sqrt{(X - X_{goal})^2 + (Y - Y_{goal})^2} \leq d^*$
Output: triggering signals $\{T_{SP}, D_{rel}\}$

traffic emergencies occur, such that the constraint (20f) should be triggered to guarantee safety. In the initialization, the triggering flag T_{SP} of the SP constraint is set as false. Subsequently, we monitor D_{rel}. If D_{ref} is less than the preset safety distance threshold D_{thold}, we set T_{SP} to true and minimize (20) under the SP constraint. Algorithm 1 stops compiling if the ego-vehicle (X, Y) reaches the goal position (X_{goal}, Y_{goal}) within a certain range of d^*.

IV. SIMULATION RESULTS

To verify the performance of the proposed SPMPC, we conducted a comparative simulation study with the latest PF-AMPC [19] using MATLAB/Simulink and CarSim in two emergency collision avoidance scenarios: i) Two-lane traffic at same direction and ii) Three-lane traffic at same direction. The parameter settings of the potential field are described in Table I, which is discussed in [11], [17]. The sampling time is 0.01 [s]. The prediction and control horizons for the MPC controller are set at 20 and 5, respectively [10], [12].

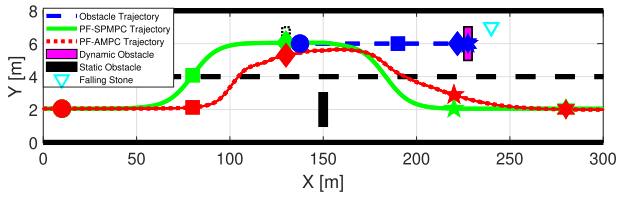

Fig. 5. Comparative ego-vehicle and obstacles' trajectories (Different shapes: positions correspond to different time points).

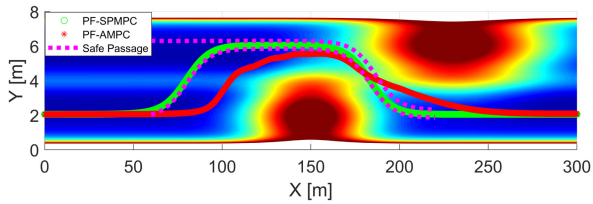

Fig. 6. Ego-vehicle trajectories with/without SP under the PF modeling at T=15 [s].

A. Scenario 1: Two-Lane Traffic

The general settings are presented in Fig. 5, where the static obstacle is set at $(X^1_{obs}, Y^1_{obs}) = (150, 2)$, and the initial position of the dynamic obstacle is set at $X^2_{obs}, Y^2_{obs}) = (130, 6)$. D_{thold} is set to 30 [m]. Note that the dynamic obstacle continues to drive at a constant speed (15 m/s) for the first 5 s of the simulation and then decelerates suddenly at 5 [m/s^2] owing to falling stones appearing in the lane.

The comparisons of the vehicle trajectories are presented in Fig. 5. Prominent oscillation can be observed in the path generated by the PF-AMPC (denoted by the red dot-solid line); such oscillation does not appear in the result for the PF-SPMPC (denoted by the green solid line) during the emergency obstacle avoidance from 120 [m] to 200 [m]. Fig. 6 shows that the potential power is rapidly enlarged due to the sudden deceleration of the dynamic obstacle when there is partial overlap with the potential field of the static obstacle from 120 [m] to 200 [m]; this leads to an undesirable gradient change. In addition, as shown by the purple dotted line computed using PF-SPMPC, the vehicle will be less affected by the sharp increase in the potential field while driving within the designed SP constraint. The comparison results for the motion states are shown in Fig. 7(a)–Fig. 7(d). We observe that the sideslip angle of PF-AMPC (red dot-solid line) reaches the empirical sideslip bound after 5 s, while that of PF-SPMPC is computed to be well within the range of $[-2.2, 3.0]$ [deg]. Furthermore, the yaw angle of PF-AMPC has local turbulence, which is maximum at about 13.1 [deg] and minimum at about -4.5 [deg] during the emergency collision avoidance. In contrast, the yaw angle of PF-SPMPC fluctuates around zero and tends to be flat within the range of $[-2.0, 0.9]$ [deg]. In Fig. 7(b), the same phenomenon can be observed: the front tire steering angle under PF-AMPC fluctuates when avoiding the decelerating dynamic obstacle and reaches the preset constraints in the range of $[-10, 10]$ [deg]. In contrast, the tire steering angle under PF-SPMPC remains well-constrained within this range.

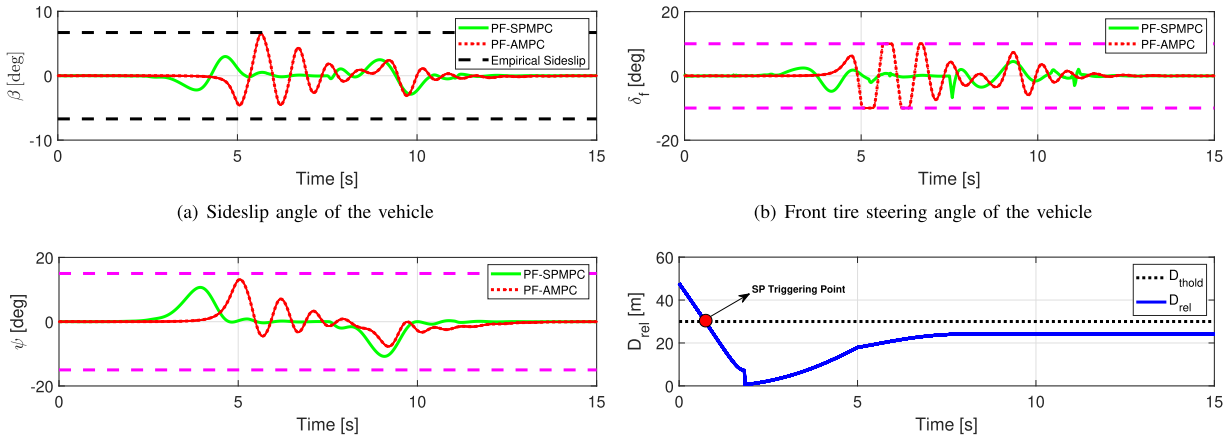

(a) Sideslip angle of the vehicle (b) Front tire steering angle of the vehicle

(c) Yaw angle of the vehicle (d) Relative distance between the two intersection points

Fig. 7. Comparative sideslip angle, front tire steering angle, and yaw angle of the ego-vehicle and relative distance between the two intersection points.

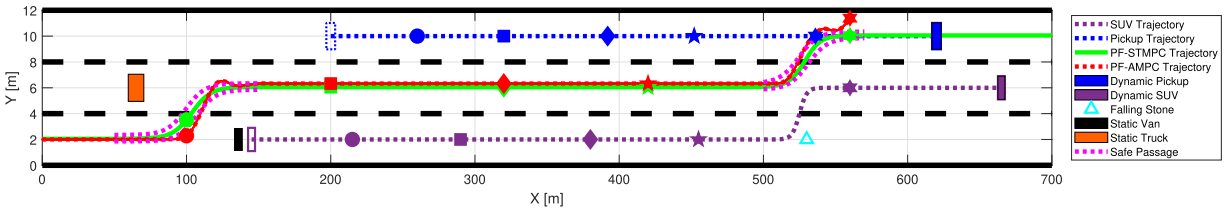

Fig. 8. Ego-vehicle and different obstacles' trajectories with/without SP constraint (Different shapes: positions correspond to different time points).

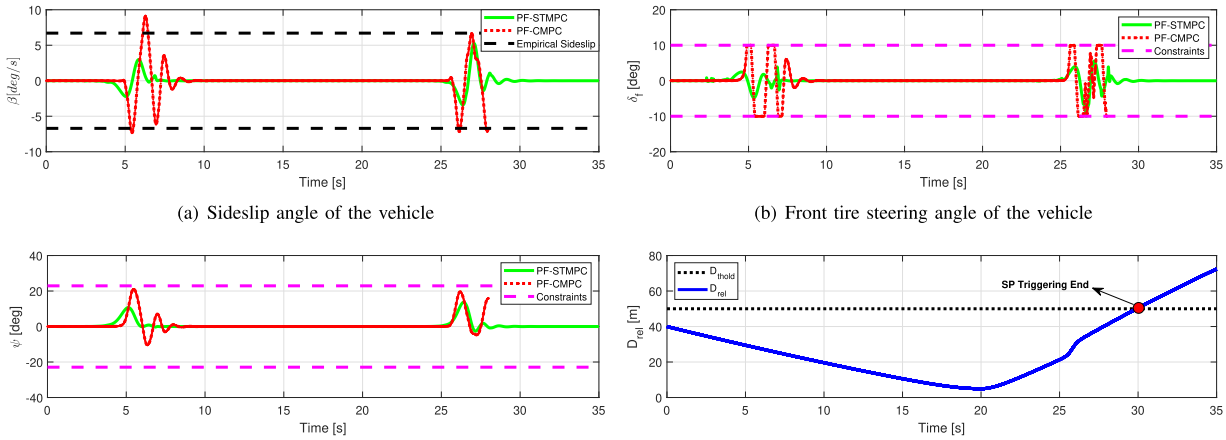

(a) Sideslip angle of the vehicle (b) Front tire steering angle of the vehicle

(c) Yaw angle of the vehicle (d) Relative distance between the two intersection points

Fig. 9. Comparative sideslip angle, front tire steering angle, and yaw angle of the ego-vehicle and relative distance between the two intersection points.

In Fig. 7(d), we can see that D_{rel} is less than the preset D_{thold} after 0.8 [s]; thus, the SP constraint is triggered at the solid red point. After 5 [s], the rate of increase in D_{rel} is reduced, and D_{rel} finally becomes constant at approximately 24.1 [m] because the dynamic obstacle vehicle stops.

B. Scenario 2: Three-Lane Traffic

In this scenario, five different cars are simulated in the three-lane traffic, including sedan (ego), SUV, van, pickup, and trailer truck. The trailer truck and van are static but closely spaced, set at (65,6) and (136,2), respectively. Pickup is set to drive at 12 [m/s], with an initial position at (200,10). The SUV is initialized at the position (145,2) with a constant speed of 15 [m/s], and then, it will suddenly swerve to simulate an emergency. The D_{thold} is set at 50 [m].

Fig. 8 depicts the result of vehicle trajectories where we can see both the PF-AMPC and PF-SPMPC can pass through the closely spaced static obstacles, but the trajectory of the PF-AMPC is steep and tortuous. Besides, the PF-SPMPC

successfully avoids the suddenly lane-changed obstacle under the SP navigation while the PF-AMPC fails to do that and hits the upper road boundary due to loss of control. From Fig. 9(a) to Fig. 9(c), we can observe from the motion states that the sideslip angle of the PF-AMPC exceeds the empirical sideslip that could cause severe yawing of the vehicle. In the contrary, the sideslip angle of the PF-SPMPC stays within the scope of empirical sideslip. Also, the front tire steering angle and yaw angle of the PF-AMPC reach the preset constraints (10 [deg] and 23 [deg]) while those of the PF-SPMPC are well-computed within the predefined constraint. In addition, excessive oscillations exist in the PF-AMPC from 5 [s] to 8.35 [s] and 25.5 [s] to 28 [s], which the PF-SPMPC does not have. In Fig. 9(d), the SP triggering estimation ends at around 30 [s] when the relative distance reaches the predefined threshold.

V. Conclusions and Discussions

Herein, we proposed a novel SP-based model predictive controller combined with a PF (PF-SPMPC) to handle emergency collision avoidance when the PFs become too unstable to plan a safe path owing to undesirable changes in the gradient descent direction during traffic emergencies. Furthermore, we compiled a triggering estimation algorithm to monitor the triggering conditions for computing the SP constraint. To verify the performance of the proposed PF-SPMPC, we compared the PF-SPMPC with the latest adaptive PF-MPC (PF-AMPC) method in MATLAB/Simulink and CarSim. The results showed that PF-SPMPC performed better than PF-AMPC in terms of finding an safe passage to eliminate the severe tire oscillations during emergency collision avoidance.

In this study, we focused on two-lane and three-lane traffics with the same driving direction. However, for applications in the real world, more challenging scenes with randomized settings should be further developed, such as oncoming traffic, signalized and non-signalized intersections, roundabouts, etc. Furthermore, the planning that considers interactions with other road users and traffic signs is promising. Several key factors, including driving styles and intentions, should be involved (cooperative/non-cooperative objects) in future work to better perform the steering/accelerating/braking maneuvers, especially in traffic emergencies like sudden changes of adjacent vehicles.

References

[1] D. Dolgov, S. Thrun, M. Montemerlo, and J. Diebel, "Path planning for autonomous vehicles in unknown semi-structured environments," *Int. J. Robot. Res.*, vol. 29, no. 5, pp. 485–501, 2010.

[2] Ö. Ş. Taş *et al.*, "Making bertha cooperate-team annieway's entry to the 2016 grand cooperative driving challenge," *IEEE Trans. Intell. Transp. Syst.*, vol. 19, no. 4, pp. 1262–1276, Apr. 2018.

[3] Y. Luo, M. Meghjani, Q. H. Ho, D. Hsu, and D. Rus, "Interactive planning for autonomous urban driving in adversarial scenarios," in *Proc. IEEE Int. Conf. Robot. Automat.*, 2021, pp. 5261–5267.

[4] K. Leung *et al.*, "On infusing reachability-based safety assurance within planning frameworks for human-robot vehicle interactions," *Int. J. Robot. Res.*, vol. 39, no. 10-11, pp. 1326–1345, 2020.

[5] D. González, J. Pérez, V. Milanés, and F. Nashashibi, "A review of motion planning techniques for automated vehicles," *IEEE Trans. Intell. Transp. Syst.*, vol. 17, no. 4, pp. 1135–1145, Apr. 2016.

[6] L. Claussmann, M. Revilloud, D. Gruyer, and S. Glaser, "A review of motion planning for highway autonomous driving," *IEEE Trans. Intell. Transp. Syst.*, vol. 21, no. 5, pp. 1826–1848, May 2020.

[7] O. Khatib, "Real-time obstacle avoidance for manipulators and mobile robots," in *Autonomous Robot Vehicles*. New York, NY, USA: Springer, 1986, pp. 396–404.

[8] P. Raksincharoensak, T. Hasegawa, and M. Nagai, "Motion planning and control of autonomous driving intelligence system based on risk potential optimization framework," *Int. J. Automot. Eng.*, vol. 7, no. AVEC14, pp. 53–60, 2016.

[9] Y. Huang *et al.*, "A motion planning and tracking framework for autonomous vehicles based on artificial potential field elaborated resistance network approach," *IEEE Trans. Ind. Electron.*, vol. 67, pp. 1376–1386, Feb. 2020.

[10] Y. Rasekhipour, A. Khajepour, and S. Chen, and B. Litkouhi, "A potential field-based model predictive path-planning controller for autonomous road vehicles," *IEEE Trans. Intell. Transp. Syst.*, vol. 18, no. 5, pp. 1255–1267, May 2017.

[11] J. Ji, A. Khajepour, W. Melek, and Y. Huang, "Path planning and tracking for vehicle collision avoidance based on model predictive control with multiconstraints," *IEEE Trans. Veh. Technol.*, vol. 66, no. 2, pp. 952–964, Feb. 2017.

[12] H. Wang, Y. Huang, A. Khajepour, Y. Zhang, Y. Rasekhipour, and D. Cao, "Crash mitigation in motion planning for autonomous vehicles," *IEEE Trans. Intell. Transp. Syst.*, vol. 20, no. 9, pp. 3313–3323, Sep. 2019.

[13] P. Lin, W. Y. Choi, and C. C. Chung, "Local path planning using artificial potential field for waypoint tracking with collision avoidance," in *Proc. IEEE 23rd Int. Conf. Intell. Transp. Syst.*, 2020, pp. 1–7.

[14] Z. Liu, X. Yuan, G. Huang, Y. Wang, and X. Zhang, "Two potential fields fused adaptive path planning system for autonomous vehicle under different velocities," *ISA Trans.*, vol. 112, pp. 176–185, 2021.

[15] P. Lin, W. Y. Choi, S.-H. Lee, and C. C. Chung, "Model predictive path planning based on artificial potential field and its application to autonomous lane change," in *Proc. 20th Int. Conf. Control, Automat. Syst.*, 2020, pp. 731–736.

[16] P. Lin, J. H. Yang, Y. S. Quan, and C. C. Chung, "Potential field-based path planning for emergency collision avoidance with a clothoid curve in waypoint tracking," in *Asian Journal of Control*. Hoboken, New Jersey, U.S.: Wiley Online Library, 2022, pp. 1–14.

[17] W. T. Michael and J. W. Burdick, "Artificial potential functions for highway driving with collision avoidance," in *Proc. IEEE Int. Conf. Robot. Automat.*, 2008, pp. 3731–3736.

[18] C. Pozna, F. Troester, R.-E. Precup, J. K. Tar, and S. Preitl, "On the design of an obstacle avoiding trajectory: Method and simulation," *Math. Comput. Simul.*, vol. 79, no. 7, pp. 2211–2226, 2009.

[19] B. Lu and G. Li, H. Wang, J. Guo, D. Cao, and H. He, "Adaptive potential field-based path planning for complex autonomous driving scenarios," *IEEE Access*, vol. 8, pp. 225294–225305, 2020.

[20] B. Paden, M. Čáp, S. Z. Yong, D. Yershov, and E. Frazzoli, "A survey of motion planning and control techniques for self-driving urban vehicles," *IEEE Trans. Intell. Veh.*, vol. 1, no. 1, pp. 33–55, Mar. 2016.

[21] B. Lu *et al.*, "Hybrid path planning combining potential field with sigmoid curve for autonomous driving," *Sensors*, vol. 20, no. 24, 2020, Art. no. 7197.

[22] Y. Koren and J. Borenstein, "Potential field methods and their inherent limitations for mobile robot navigation," in *Proc. IEEE Int. Conf. Robot. Automat.*, 1991, vol. 2, pp. 1398–1404.

[23] C. Sierra and E. Tseng, A. Jain, and H. Peng, "Cornering stiffness estimation based on vehicle lateral dynamics," *Veh. Syst. Dyn.*, vol. 44, no. sup1, pp. 24–38, 2006.

[24] S. Fahami and H. Zamzuri, and S. Mazlan, "Development of estimation force feedback torque control algorithm for driver steering feel in vehicle steer by wire system: Hardware in the loop," *Int. J. Veh. Technol.*, Hindawi, vol. 2015, pp. 1–17, 2015.

[25] R. Rajamani, *Vehicle Dynamics and Control*. New York, U.S.: Springer, 2011.

[26] S. Shalev-Shwartz, S. Shammah, and A. Shashua, "On a formal model of safe and scalable self-driving cars," 2017, *arXiv:1708.06374v6*.

[27] B. Gassmann *et al.*, "Towards standardization of AV safety: C library for responsibility sensitive safety," in *Proc. IEEE Intell. Veh. Symp.*, 2019, pp. 2265–2271.

[28] I. R. Shafarevich and A. O. Remizov, *Linear Algebra and Geometry*. London, England, Springer, 2012.

[29] X. Zheng and P. Palffy-Muhoray, "Distance of closest approach of two arbitrary hard ellipses in two dimensions," *Phys. Rev. E*, vol. 75, no. 6, 2007, Art. no. 061709.